Optimal placement of microphones and piezoelectric transducer actuators for far-field sound radiation control

Bor-Tsuen Wang
Department of Mechanical Engineering, National Pingtung Polytechnic Institute, Pingtung, Taiwan 91207, Republic of China

(Received 21 August 1995; accepted for publication 15 December 1995)

This paper presents an optimization solution technique to determine the optimal locations of piezoelectric transducer (PZT) actuators and far-field microphone sensors for active structural acoustic control in conjunction with the use of least-mean-square (LMS) feedforward control algorithm. A simply supported beam in an infinite rigid baffle subject to an harmonically excited point force is considered. The piezoceramic patches are adhered to the beam and act as control transducers, while microphones located in the far field are used as error sensors. The objective function is first defined as the total radiated sound power. The design variables which are the locations of PZT actuators and microphone sensors are then identified and determined. The genetic algorithm (GA) incorporated with the use of linear quadratic optimal control theory (LQOCT) to calculate the control voltages to the actuators is adopted to solve the optimization problem. Results show that the optimally placed PZT actuators and microphone sensors can perform better sound radiation control than the arbitrarily selected ones. In particular, for off-resonance excitation cases the optimized PZT actuators and microphone sensors can efficiently control the sound radiation and eliminate the control spillover. The control mechanisms of PZT actuators and microphone sensors are demonstrated through the studies of radiation directivity patterns and beam displacement distributions as well as the wave-number analysis. The effect of the number of microphone sensors are also presented. The use of optimally positioned PZT actuators and microphone sensors can efficiently achieve structural sound radiation control. © *1996 Acoustical Society of America.*

PACS numbers: 43.40.Vn, 43.38.Fx, 43.40.Cw, 43.40.Rj

INTRODUCTION

Structural sound radiation control is of a great deal of interest. Either vibrational control forces, such as shakers[1,2] and distributed types of actuators,[3–5] or acoustical control sources, such as loudspeakers,[6–9] can be applied to reduce structural sound radiation. Acoustical error sensors like microphones[6,10,11] are generally used as control sensors directly measuring the sound-pressure response in the acoustic field. Because of the structure/acoustic interaction, structural motions are strongly coupled into the acoustic response. Vibration error sensors, such as accelerometers[12,13] and distributed types of sensors,[14–18] can also be used in active structural acoustic control.

The location of actuators and sensors can strongly affect the system behavior and is of a great deal of concern.[13,19–24] Fuller and Jones[19] have shown the influence of vibration control force and microphone location on the performance of interior noise control. They claimed that the vibrational control actuator should be located near the antinodes of the modes to be controlled, while the microphone sensor should be placed where the response of all modes to be controlled is strong. Naghshineh[13] presented a rational procedure for selecting the number and location of vibrational control forces and accelerometers by using acoustic basis functions instead of one based on the response of the structure. He demonstrated that placing actuators at the antinodes of the highest-order acoustic basis function is superior to placing actuators at antinodes of the structural vibration modes, while vibration error sensors coincide to actuators. Bullmore *et al.*[20] studied the active minimization of harmonic enclosed sound fields by using a single secondary sound source in conjunction with the use of a number of discrete microphones. They found that the secondary sound source located at a maximum of the primary sound field can provide substantial reduction of the acoustic potential energy. The microphone's error sensors should be placed at the corners of the enclosure where a maximum of any mode shape is always detected.

Distributed types of actuators and sensors, such as PZT actuators and PVDF sensors, can be potentially used as control transducers. Previous research has analytically and experimentally demonstrated their applications to structural vibration[25–29] and sound radiation control.[3,4,14–16,30,31] Dimitriadis *et al.*[28] suggested that the optimum boundaries of the PZT actuator can be along nodal lines or the boundaries of plates for efficient excitation. Jia[32] showed that by maximizing the length of the PZT actuator covering a whole lobe of the structure mode shape to be controlled can effectively suppress the single mode response of the beam vibration. Recent studies[23,24] presented a solution strategy by using the gradient search method for the nonlinear optimization problem regarding to the optimal placement of the PZT actuators and PVDF sensors. Wang *et al.*[23] found that the optimal location of finite length of PZT actuators are away from the nodal line in contrast to the suggestion from Dimitriadis *et al.*,[28] because the optimal location of actuators is determined upon a compromise between equally reduce several plate modes instead of just one. To formulate the optimization problem, the objective function to be minimized is gen-

 0001-4966/96/99(5)/2975/10/$6.00

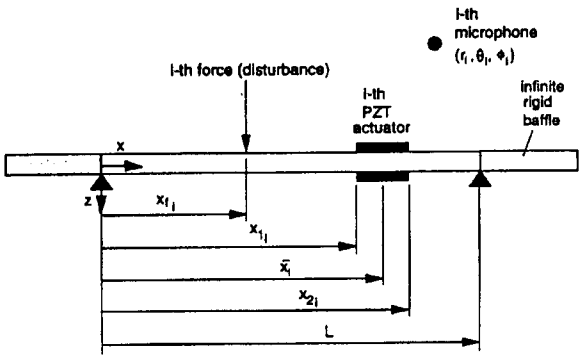

FIG. 1. The arrangement of coordinates of simply supported beam.

erally defined as the total radiated power or approximated by the sum of a number of discrete pressure sensors and is a multiminimum nonlinear function. When applying the gradient search method, selecting the initial guess can be critical to the optimal solution. Additionally, computer simulation is a complicated task and requires a large computing effort for calculating the gradients. A more efficient solution technique may be required. The genetic algorithm (GA) which is a simple algebraic procedure has been widely applied to various types of optimization problems.[33–35] Wang[36] developed a solution technique based on the GA to determine the optimal location of vibrational control forces and accelerometers for structural vibration control. This work utilizes the analysis technique to determine the optimal placement of PZT actuators and microphone sensors for controlling far-field sound radiation from structures.

This paper considers a simply supported beam mounted in an infinite rigid baffle subjected to a harmonic point force disturbance. While microphones are used as far-field error sensors, the piezoceramic patches are implemented as control actuators in conjunction with the use of LMS feedforward control. A solution strategy adopting the GA in conjunction with the use of linear quadratic optimal control theory (LQOCT) is proposed to determine the optimal location of PZT actuators and microphone sensors. Both on- and off-resonance excitation cases are presented to demonstrate the control mechanism and performance of PZT actuators and microphone sensors. Results show that the optimally placed PZT actuators and microphone sensors show much better sound radiation control than those arbitrarily chosen. In particular, for off-resonance excitation the optimally positioned actuators and sensors can significantly achieve efficient sound radiation control in comparison with the arbitrarily selected ones. This work provides an optimum design methodology for positioning actuators and sensors in active structural acoustic control.

I. THEORETICAL ANALYSIS

A. Sound radiation from the beam

The sound pressure radiating to the far-field from a simply supported beam in an infinite rigid baffle shown in Fig. 1 can be derived from the Rayleigh integral as follows:[37]

$$p(r,\theta,\phi,t)=e^{i\omega t}\sum_{n=1}^{\infty} W_n q_n, \tag{1}$$

where

$$W_n=\frac{P_n}{\rho_b b t_b(\omega_n^2-\omega^2)}, \tag{2}$$

$$q_n=-i\omega\,\frac{\rho c b}{\pi}\,\frac{\kappa}{\alpha_n}\,\frac{e^{-i\kappa r}}{2r}\left[\frac{1-(-1)^n e^{-i\alpha}}{1-(\alpha/n\pi)^2}\right]\left[\frac{1-e^{-i\beta}}{\beta}\right], \tag{3}$$

$$\omega_n=(n\pi)^2\sqrt{E_b I/\rho_b b t_b L^4}, \tag{4}$$

$$\alpha_n=n\pi/L, \tag{5}$$

$$\alpha=\kappa L\,\sin\,\theta\,\cos\,\phi, \tag{6}$$

$$\beta=\kappa b\,\sin\,\theta\,\sin\,\phi. \tag{7}$$

Here, E_b is the Young's modulus of the beam, I is the moment of inertia, ρ_b is the beam density, t_b is the beam thickness; b is the beamwidth, ρ is the air density, c is the sound speed in air, κ is the acoustic wave number, and P_n is the modal force depending on the form of excitation. For a harmonic point force with the amplitude of F located at x_f acting on the beam, the modal force, P_n^f, is given as follows:

$$P_n^f=(2F/L)\sin\,\alpha_n x_f. \tag{8}$$

For an actuator consisting of two identical piezoceramic patches bonded symmetrically on the two opposite beam surfaces and activated 180° out-of-phase, the equivalent external forces are the concentrated moments acting on both edges of piezoceramic patches. The corresponding expression of modal force for piezoelectric excitation, P_n^c, can be derived[38] as follows:

$$P_n^c=(2M_{eq}/L)\alpha_n(\cos\,\alpha_n x_1-\cos\,\alpha_n x_2), \tag{9}$$

where

$$M_{eq}=(t_b^2 E_b/6+\Psi)b_a\Lambda, \tag{10}$$

$$\Psi=E_b t_b/E_a t_a, \tag{11}$$

$$\Lambda=(d_{31}/t_a)V, \tag{12}$$

where M_{eq} is the equivalent moment induced by the piezoelectric patches attached to the top and bottom of the beam and excited 180° out-of-phase, Λ is the strain induced by an unconstrained piezoelectric layer of thickness, t_a, when a voltage V is applied along its polarization direction, while d_{31} is the piezoelectric dielectric strain constant and Ψ is the effective stiffness ratio.[25] The resultant force is, in fact, the concentrated moments acting on the both edges of piezoelectric patches. Here, x_1 and x_2 are the coordinates of the piezoelectric actuator.

Under the assumption of superposition, the total radiated sound pressure can be the sum of sound pressures due to the disturbance and control inputs

$$p_t=p_f+p_c=e^{i\omega t}\sum_{n=1}^{\infty}(W_n^f+W_n^c)q_n. \tag{13}$$

The total radiated sound power defined as the integral of the square of the radiated sound pressure over the hemisphere of the radiating field can then be obtained as

$$\Phi_p=\frac{1}{2\rho c}\int_S |p_t|^2\,dS$$

$$=\frac{r^2}{2\rho c}\int_0^{2\pi}\int_0^{\pi/2}|p_t|^2\sin\theta\,d\theta\,d\phi. \tag{14}$$

The total radiated sound power can be used as an index to evaluate the effectiveness of sound radiation control and can be chosen as the objective function for the purpose of optimization.

B. Wave-number analysis

The beam velocity transform can be obtained by performing Fourier integral transform and can be expressed as:[31]

$$\tilde{V}(\kappa_x,\kappa_y)=i\omega\sum_{n=1}^{\infty}W_nV_n, \tag{15}$$

where

$$V_n=i\alpha_n\left[\frac{1-(-1)^n e^{-i\kappa_x L}}{\alpha_n^2-\kappa_x^2}\right]\left[\frac{e^{-i\kappa_y b}-1}{\kappa_y}\right], \tag{16}$$

$$\kappa_x=\kappa\sin\theta\cos\phi, \tag{17}$$

$$\kappa_y=\kappa\sin\theta\sin\phi. \tag{18}$$

It is noted that the mean-square value of the velocity wave-number transform, i.e., $|\tilde{V}|^2$, integrated over the supersonic region is proportional to the radiated sound power.[39] Only the wave-number components satisfying $\kappa_x^2+\kappa_y^2<\kappa^2$ contribute to sound radiation into the far field and are termed as supersonic waves. The remaining wave-number components are associated with subsonic waves and therefore do not radiate into the far field.

C. Linear quadratic optimal control theory

For sound radiation control, microphones located in the far field are generally used as error sensors. For the use of N_m microphone sensors, the cost function can be defined as the sum of the mean-square value of the sound pressures measured from the microphones:

$$\Psi_p=\sum_{j=1}^{N_m}|p_t(r_j,\theta_j,\phi_j)|^2. \tag{19}$$

The linear quadratic optimal control theory (LQOCT) can then be applied to minimize the cost function so as to find the optimal control voltages input to the piezoelectric actuators. The full analysis can be referred to the work of Wang[40] and omitted here for brevity.

D. Genetic algorithm

The genetic algorithm is derived based on Darwin's theory of "survival of the fittest."[33] The GA is a search procedure for general optimization problems and is numerically simple involving nothing more than random number generation, bit manipulation and string exchange. The objective function is usually transformed to a fitness function

$$F(x)=\text{base value}-f(x). \tag{20}$$

The GA is to maximize the fitness function $F(x)$ in contrast to minimize the objective function $f(x)$ in comparison with the traditional optimization procedures. The design variables x, are encoded as a binary digit string which is analogous to chromosome in a biological system. When multiple design variables are desired, all design variables are concatenated to one single string. In the beginning, the GA randomly generates a population of strings by successive coin flips. The generation process is then succeeded to produce the new generation of population by performing three basic operators of GA: reproduction, crossover, and mutation. Strings can be decoded to obtain the exact values of the design variables in order to calculate the fitness values. The design constraints can be treated by the exterior penalty function method such that a constrained problem is transformed to an unconstrained problem.

E. Formulation of optimization problem

As shown in Fig. 1, a simply supported beam in an infinite rigid baffle is considered as the plant subjected to a harmonically excited point force disturbance. The sound radiation from the beam is controlled by PZT actuators in conjunction with the use of LMS feedforward control algorithm, while the far-field microphones are used as the error sensors. The size of the ith PZT actuator is assumed to be fixed. The applied voltages to the piezoelectric actuators can be calculated from linear quadratic optimal control theory (LQOCT). Therefore, the design variables can be identified as

$$\bar{x}_1,\bar{x}_2,\ldots,\bar{x}_{N_c},r_1,r_2,\ldots,r_{N_m},\theta_1,\theta_2,\ldots,\theta_{N_m},\phi_1,\phi_2,\ldots,\phi_{N_m}, \tag{21}$$

where $\bar{x}_i$ are the central location of the ith PZT actuator, and (r_i,θ_i,ϕ_i) are the coordinates of the ith microphones respectively as illustrated in Fig. 1. To simplify the problem, the radial distance and rotational angle are assumed to be fixed as $r_i=3$ m and $\phi_i=0°$. The angle θ_i, is assumed to be in the range of $-90°<\theta_i<90°$, i.e., the microphone is right above and parallel to the longitudinal direction of the beam. When θ_i is negative, the microphone is at $\phi_i=180°$. Therefore, the design variables can be reduced to

$$\bar{x}_1,\bar{x}_2,\ldots,\bar{x}_{N_c},\theta_1,\theta_2,\ldots,\theta_{N_m}. \tag{22}$$

The objective function can then be defined as the total radiated sound power as shown in Eq. (14) and transformed to a fitness function as shown in Eq. (20). The bounds of design variables can be inherently implemented, and the unconstrained optimization problem can be completely defined. Therefore, the genetic algorithm can then be applied to determine the optimal locations of PZT actuators and microphone sensors. The solution strategy is described as follows.

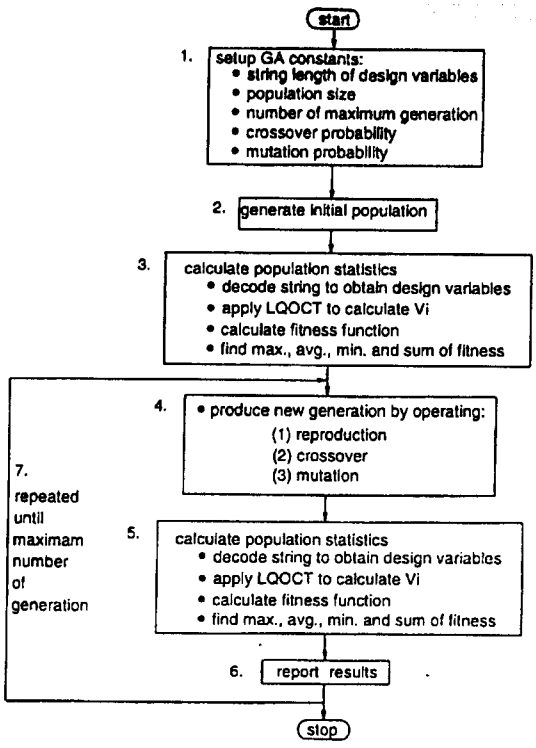

FIG. 2. Flow chart of solution strategy.

II. SOLUTION STRATEGY

A. Implementation of genetic algorithm

The GA is implemented as FORTRAN codes incorporated with the use of LQOCT for the calculation of the optimal control voltages input to actuators whenever the locations of actuators and sensors are determined. The solution flow chart is shown in Fig. 2. The detail procedure is described as follows.

(1) Set up GA constants. At the beginning of the program, some GA constants including population size for each generation, the string length of design variables, crossover probability, mutation probability and the number of maximum generation must be specified.

(2) Generate initial population. The binary digit string is generated by successive coin flips. The design variables are encoded as a binary digit string. All design variables are concatenated to one single string.

(3) Calculate the population statistics. In this stage, each string is decoded to obtain the exact values of design variables, which are the central locations of PZT actuators and the radial angles of microphone sensors. The LQOCT is then applied to calculate the control voltages input to the PZT actuators for each one string contained in the populations. The fitness function for each string can also be computed. Finally, the maximum, averaged, minimum and sum of the fitness for the current generation can be obtained. Those values are required in the production of new generation.

(4) Produce new generation. To produce a new generation, three basic GA operators, i.e., reproduction, crossover and mutation, are performed. A pair of reproduction mates are first selected by a roulette wheel with slots sized according to the fitness values. The crossover is then performed for the selected reproduction mates based on the crossover probability. Finally, the mutation is performed on the children sets to produce the new generation array.

(5) Calculate the population statistics. The procedures are the same as those in step 3.

(6) Report results. This stage is to print out the results of population statistics as well as the string digit and the exact values of design variables for further analysis.

(7) Repeat steps 4 to 6 until the program reaches the number of maximum generation.

B. Design processes

To determine the optimal locations of PZT actuators and microphone sensors, two design processes are taken. First, the locations of microphone sensors are assumed to be fixed, only the locations of PZT actuators are to be optimized. Second, when the optimal locations of the PZT actuators are obtained from design process I and assumed to be fixed, the locations of microphone sensors are then optimized. One can also solve for the optimal locations of actuators and sensors simultaneously. Only more design variables are involved in the optimization process and it therefore results in a larger solution combinations. More population size or more generations may be required to obtain satisfactory solutions. In this paper, only design processes I and II are considered, which demonstrate the applicability of GA to determine the optimal location of actuators and sensors.

C. Selection of GA parameters

To successfully obtain the optimal solution by GA, one should carefully select the GA parameters, such as population size, mutation probability, and crossover probability. According to De Jong's study,[38] he suggested that a high-crossover probability, a low-mutation probability, and a moderate population size can be required for satisfactory performance. This suggestion is useful for general application to optimization problems. In particular, to decide the parameter values one should fully understand the characteristics of the objective function to be optimized. Generally speaking, the GA involving algebraic operation is much simpler than other optimization methods which require the evaluation of the gradients of objective functions. Wang *et al.*[23] indicated that approximately over 70%–90% of the computing effort contributes to the calculation of the gradients. In the case of optimal placement of actuators and sensors in ASAC, the objective function is defined as the total radiated sound power which involves an integration as shown in Eq. (14). Therefore, a moderate population size must be carefully selected in order to obtain the optimum without increasing the computing effort. In the following numerical simulations, the population size is assumed to be 20 for one design variable, 40 for two design variables, etc.

The effects of mutation and crossover probabilities on the GA performance is also a great concern. The optimization of a simple quadratic function by varying mutation and

TABLE I. Natural frequencies of the simply supported beam.

Mode	Frequency (Hz)
1	33.2
2	128.8
3	289.9
4	515.4
5	805.3
6	1159.6
7	1578.3
8	2061.4
9	2609.0
10	3220.9

TABLE II. Physical properties of the G-1195 piezoceramic patch.[42]

$E_a=6.3\times10^{10}(\mathrm{N/m^2})$	$\rho_a=7650\ (\mathrm{kg/m^3})$
$t_a=1.905(\mathrm{mm})$	$\nu_a=0.28$
$d_{31}=d_{32}=166\times10^{-12}(\mathrm{m/V})$	

crossover probabilities has been studied.[41] For small mutation probabilities, the convergence rate can be low. This may require more generations to obtain the optimum. For higher mutation probabilities, the maximum fitness value may be obtained in the earlier generation. However, the averaged fitness value may be relatively low. The effect of crossover probability is primarily on the initial generation. In terms of the maximum fitness value, the smaller the crossover probability, the higher the convergence rate, and vise versa. Upon the consideration of convergence rate and computing efficiency, the number of maximum generation is set to be ten, and the crossover and mutation probabilities are set to be 0.6 and 0.02, respectively. Each design variable is coded by a ten digit string which consists of $2^{10}=1024$ combinations of solutions such that the location accuracy is about 0.4 mm, and the angle accuracy is about 0.175°.

III. ANALYTICAL RESULTS

A steel beam with length of 0.38 m, width of 0.04 m, and thickness of 2 mm is used in the simulations. Table I shows the natural frequencies of the simply supported beam. It is noted that no damping was included in the following analysis. A harmonic point force with input parameters, $F=0.3\ N$ and $x_f=0.067$ m, was considered for the following analysis. The physical properties of the piezoelectric patch (G-1195)[42] are shown in Table II. The length of PZT actuators is assumed to be 0.0635 m. For design process I, the microphone is assumed to be located at $(r,\theta,\phi)=(3m,45°,180°)$. For the purpose of comparison, an arbitrary set of PZT actuator and microphone sensor is chosen. The piezoceramic patch is located at $x_1=0.285$ m, $x_2=0.3485$ m, and the microphone is located at $(r,\theta,\phi)=(3m,45°,180°)$. In order to calculate the beam response and radiated sound pressure, it was necessary to truncate the modal sums in Eq. (1). Upon consideration of computing time and accuracy, the first ten modes were considered, and it was found to provide sufficient convergence of series.

Both the radiation directivity and beam displacement distributions were shown to demonstrate the control mechanisms of sound radiation from the beam. The radiated sound pressure is plotted in dB *re*: 20×10^{-6} Pa over $\theta=-90°$ to 90° for $\phi=0°$ at a radial distance of 3 m from the beam, which is well into the far field. The beam displacement distribution is normalized by the largest amplitude in each case and plotted in logarithmic scale along the beamlength. The mean square values of velocity transform are also plotted along the structural wave number κ_x in logarithmic scale, when $\kappa_y=0$.

A. Optimal location of PZT actuators and microphones

Assuming that the microphone is located at (3 m, 45°, 180°), the locations of PZT actuators are to be optimized by the GA. The optimal locations of PZT actuators can be found and listed in Table III denoted by $1A_0/1S$. The PZT actuators are depicted in Fig. 3, and the associated structural mode shapes are also shown. For the 33-Hz excitation case, i.e., near the first resonance mode, one edge of the PZT actuator is close to the maximum response of the first structural mode shape. For 129- and 290-Hz excitation cases, i.e., near the second and the third resonance modes, respectively, one edge of the PZT actuator is near to the nodal point of the associated structural mode shapes. This agrees with the suggestion of Dimitriadis *et al.*,[28] because a single mode dominates the sound radiation. The finite length of PZT actuator is considered here in contrast to maximizing the length of PZT actuator covering a whole lobe of the structure mode shape as shown by Jia.[32] The PZT actuator location is determined under a compromise to eliminate the significant modes. For example, in the 80-Hz excitation case, the optimal PZT actuator is neither centrally located over the lobe of the first or the second structural mode shape. Instead, the PZT actuator is located somewhere between the maximum response of the first and the second structural mode shapes which are the significant modes.

Assuming that the optimized PZT actuator is to be fixed and one microphone is applied as the far-field error sensor, the microphone location is then optimized. For the purpose of comparison, the microphone is assumed to be located in

TABLE III. Optimal location of PZT actuators and microphone sensors.

Excitation frequency (Hz)	$1A_0/1S$ x_1,x_2	$1A_0/1S_0$ θ_1	$1A_0/2S_0$ θ_1,θ_2	$1A_0/3S_0$ $\theta_1,\theta_2,\theta_3$
33	0.12313,0.18663	−0.08°	89.64°,−85.57°	20.67°,31.23°,−62.02°
80	0.12313,0.18663	−0.08°	79.09°,−78.56°	57.97°,−29.64°,−22.08°
129	0.11478,0.17828	41.26°	14.16°,−28.59°	90.00°,−50.76°,−68.35°
210	0.24472,0.30802	34.39°	−3.78°,−35.80°	23.48°,32.63°,−19.09°
290	0.06528,0.12878	−0.08°	18.91°,−42.84°	29.64°,−16.80°,−80.32°

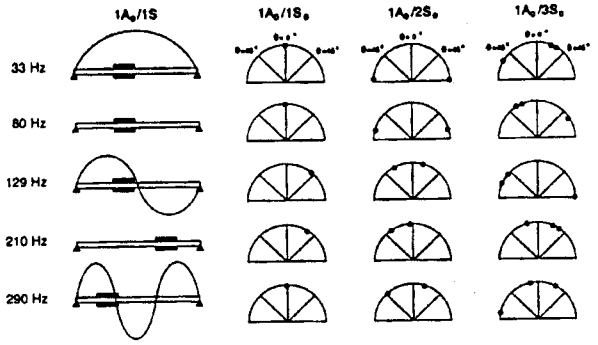

FIG. 3. Optimal locations of PZT actuators and microphone sensors.

the range of $-90°<\theta<90°$, when $\phi=0°$. The optimal location of the microphone can be determined as listed in Table III and depicted in Fig. 3 denoted by $1A_0/1S_0$. For the first and third resonance excitation, i.e., 33- and 290-Hz excitation cases, the optimal microphone is located right on the top of the beam where the maximum sound-pressure response is. This agrees with previous works.[19,20] The microphone sensors should be placed where the responses of all modes to be controlled is maximum. For the second resonance excitation, the microphone is to be located at $\theta=41°$. The microphone location is optimized such that the first and second modes, which are the most significant radiation modes, can be efficiently controlled. As shown in Table IV, the modal amplitudes are reduced by 8.5 dB for the first mode and 65.8 dB for the second. For the case of off-resonance excitation at 80 Hz, i.e., between the first and second resonance modes, the optimal location of the microphone is the same as that for the first resonance excitation case, because the sound-pressure response is also dominated by the first mode. For the 210-Hz excitation case, the microphone is at $\theta=34°$ whose location is also determined under a comprise to eliminate the significant radiation modes.

B. The effects of number of microphone sensors

It is also interesting to know where the optimal location of microphones will be and how well the sound radiation control can be achieved, if the same optimized PZT actuator is used, and two or three microphones are applied as error sensors. For applying two and three microphones as error sensors, their optimal locations are listed in Table III and depicted in Fig. 3 denoted by $1A_0/2S_0$ and $1A_0/3S_0$, respectively. For the cases of $1A_0/2S_0$ excitations at 33, 80, and 129 Hz, the microphone is about symmetrically located at both sides of the central line of the beam. In particular, the microphones are nearly closed to the baffle for the first resonance excitation case such that the sound pressure can be equally reduced at these locations resulting in the maximum reduction of sound radiation. For applying three microphones, the optimal locations of microphones distribute widely over the half-circle. For the 33- and 80-Hz excitation cases in which the first radiation mode dominates the far-field sound radiation, one can see that the microphones are located at a mirror image of each other, because of the symmetry of the first radiation mode shape.

TABLE IV. Reduction of modal amplitude (dB) for $1A_0/1S_0$.

Excitation frequency (Hz)	$n=1$	$n=2$	$n=3$	$n=4$	$n=5$
33	56.4	10.5	−11.8	−19.4	−7.3
80	16.5	19.5	−10.8	−19.2	−5.3
129	8.5	65.8	−7.5	−16.7	−14.1
210	−2.2	19.1	−5.6	−5.9	−18.8
290	2.5	13.3	62.8	−1.6	−18.2

TABLE V. Reduction of the total radiated power (dB).

Excitation frequency (Hz)	$1A_0/1S$	$1A_0/1S_0$	$1A_0/2S_0$	$1A_0/3S_0$	Arb.
33	46.2	72.8	73.5	78.0	26.1
80	21.2	47.6	47.3	47.3	0.8
129	44.2	52.1	65.3	65.7	18.6
210	10.2	16.4	16.7	16.8	−2.7
290	46.7	71.6	72.3	74.9	26.7

Table V summarizes the reduction of total radiated sound power for all of the cases. A significant amount of radiated sound power can be reduced for the optimization cases. An arbitrary set of PZT actuator and microphone sensor denoted by "Arb." is also shown for comparison. The arbitrarily selected PZT actuator and microphone sensor can achieve sufficient sound radiation control for on-resonance excitation; however, control spillover may occur for off-resonance excitation. Here, the optimized PZT actuator and microphone sensor can provide better sound radiation control and, in particular, reduce the control spillover for off-resonance excitation. For the cases of $1A_0/1S_0$, i.e., the PZT actuator and microphone sensor are optimized, the reduction of total radiated sound power is much higher than that for the cases of $1A_0/1S$ in which only the PZT actuator is optimized. When the number of error microphones is increased for applying one PZT actuator, not much improvement can be made; however, the microphone locations can be varied. The control mechanisms are also different and will be shown in the following presentations of radiation directivity patterns and beam displacement distributions as well as the wave-number analysis.

Figure 4 shows the radiation directivity patterns for the cases of $1A/1S_0$, $1A_0/1S_0$, and "Arb." For the 33-Hz excitation case as shown in Fig. 4(a), the solid line represents sound-pressure response due to the disturbance and reveals a uniform monopole response as expected. For applying the arbitrarily selected actuator and sensor, the sound pressure is largely reduced and there appears a dip at $\theta=45°$ where the microphone is positioned, because the LMS feedforward control algorithm tends to minimize the response at the sensor location. Generally speaking, sound radiation can be well controlled except in the cases of off-resonance excitation for "Arb." As shown in Fig. 4(b) and (d) for the "Arb." cases, the sound pressure near the location of the microphone can be reduced; however, sound radiation may have control spillover to the other radiation angles. For the optimization cases, sound-pressure level can be further reduced, and a different radiation shape will appear due to the different mi-

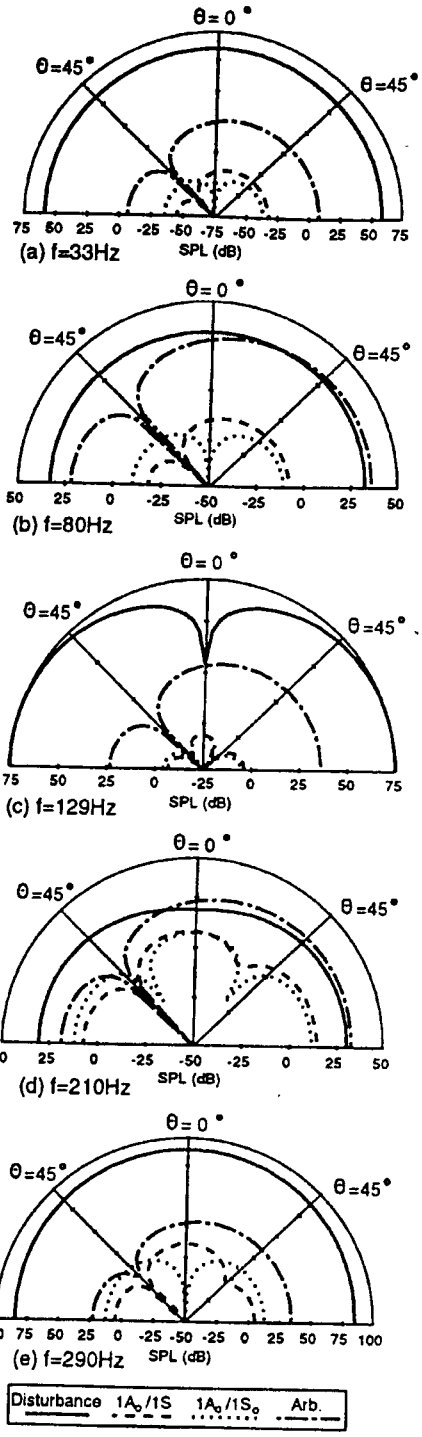

FIG. 4. Radiation directivity patterns for one microphone.

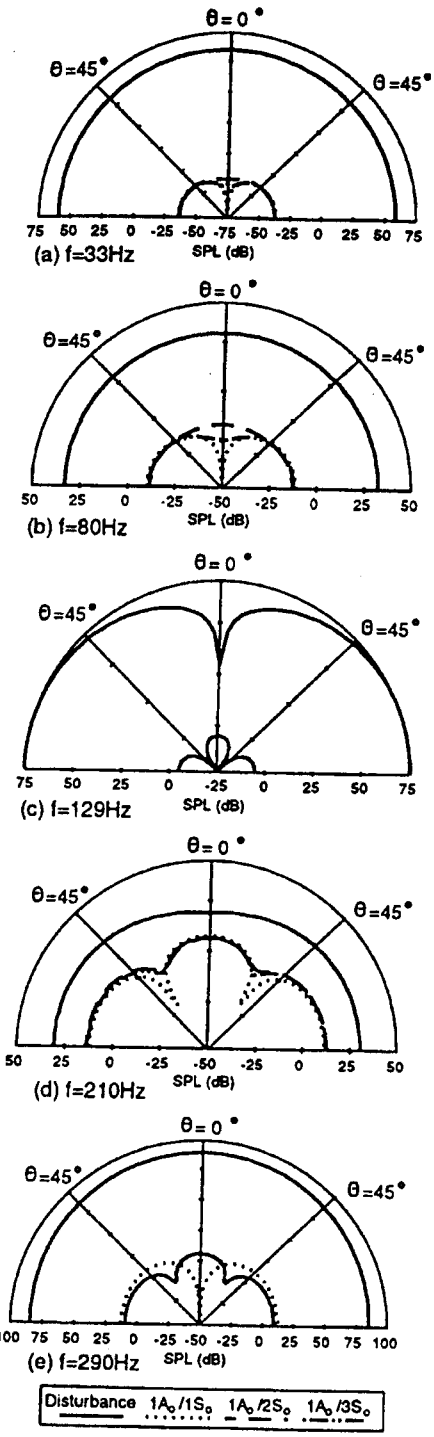

FIG. 5. Radiation directivity patterns for multiple microphones.

crophone location. For the case of $1A_0/1S$, the sound-pressure response has a dip at $\theta=45°$ where the microphone is located. For the case of $1A_0/1S_0$, the residual sound-pressure response has a dipole response for excitations at 33, 80, and 290 Hz because of the optimal microphone location at $\theta=0°$. The residual sound-pressure responses appear like the third radiation mode shapes for excitations at 129 and 210 Hz, because the microphones are located at $\theta=41.26°$ and $\theta=34.39°$, respectively, as shown in Table III.

To further examine the control mechanisms and performance for applying multiple microphones as the error sensors, Fig. 5 shows the radiation directivity patterns for the

cases of $1A_0/1S_0$, $1A_0/2S_0$, and $1A_0/3S_0$. For applying multiple microphones and only one PZT actuator, the reduction of radiated sound power is about the same as shown in Table V; however, their residual sound pressure response may be different. For the 290-Hz excitation case, the residual sound-pressure response for the case of $1A_0/1S_0$ reveals a dipole response, because the sound pressure at the microphone position can be driven to zero as one PZT actuator is applied in conjunction with the use of LMS feedforward control algorithm. The residual sound-pressure responses for $1A_0/2S_0$ and $1A_0/3S_0$ shows the third radiation mode shapes, because the sound pressure at the locations of microphones are equally reduced and cannot be driven to zero by applying only one actuator. It is also noted that for the 129-Hz excitation the residual directivity patterns appear almost the same when applying one, two, and three microphones. It is because the microphones are restrained to be located in the half-circle as shown in Fig. 3. For practical applications, one can easily utilize the developed optimization technique to determine the microphone location for any radiation angle including θ_i and ϕ_i simultaneously.

It is also interesting to examine the beam displacement distributions and study their relation with structural sound radiation. Figure 6 shows the beam displacement distributions corresponding to the cases in Figs. 4 and 5. The thin solid line represents the response due to the disturbance. For on-resonance excitation cases applying control, the beam displacement can be globally reduced. For example, for the 33-Hz excitation case as shown in Fig. 6(a) the residual beam displacement can appear like the third structural mode shape which is a less efficient radiation mode. Notice that for the optimization cases the residual beam displacement distributions also show the similar vibration mode shapes. It is because the PZT actuators can directly affect the beam response, and the control voltages of the PZT actuators for optimization cases are about the same as shown in Table VI. Therefore, the resulting vibration responses can be similar to each other. On the other hand, the different directivity patterns as shown in Fig. 5(a) imply that the locations of microphone sensors do affect the sound-pressure response in the far field. It is also noted that for the optimization cases excitation at the 210 Hz the beam displacements are increased as shown in Fig. 6(d); however, the total radiated sound power is reduced about 16 dB as shown in Table V. The residual beam responses are reformed as the third structure mode shape resulting in the third radiation mode shape as shown in Fig. 5(d). This can be further explained that the significant radiation modal response, here the second mode, is controlled leaving the less significant radiation mode, the third mode. This can be evidenced by Table IV in which for the 210-Hz excitation case the second modal amplitude is reduced by 19.1 dB, and the third one is increased by 5.6 dB.

It is also interesting to study the mean square values of velocity transform in the wave-number domain as shown in Fig. 7. The thin solid line represents the response due to the disturbance. For the "Arb." case, the residual response of $|\tilde{V}|^2$ shows a dip at $\kappa_x = \kappa \sin\theta\cos\phi$, because the sound pressure at this radiation angle is reduced to zero. The wave-number components can be globally reduced for on-resonance cases and have a different shape. For off-resonance cases, some wave-number components are increased in the supersonic region, i.e., $-\kappa < \kappa_x < \kappa$; therefore, control is not effective. For the optimization cases, the mean square values of velocity transform can be further re-

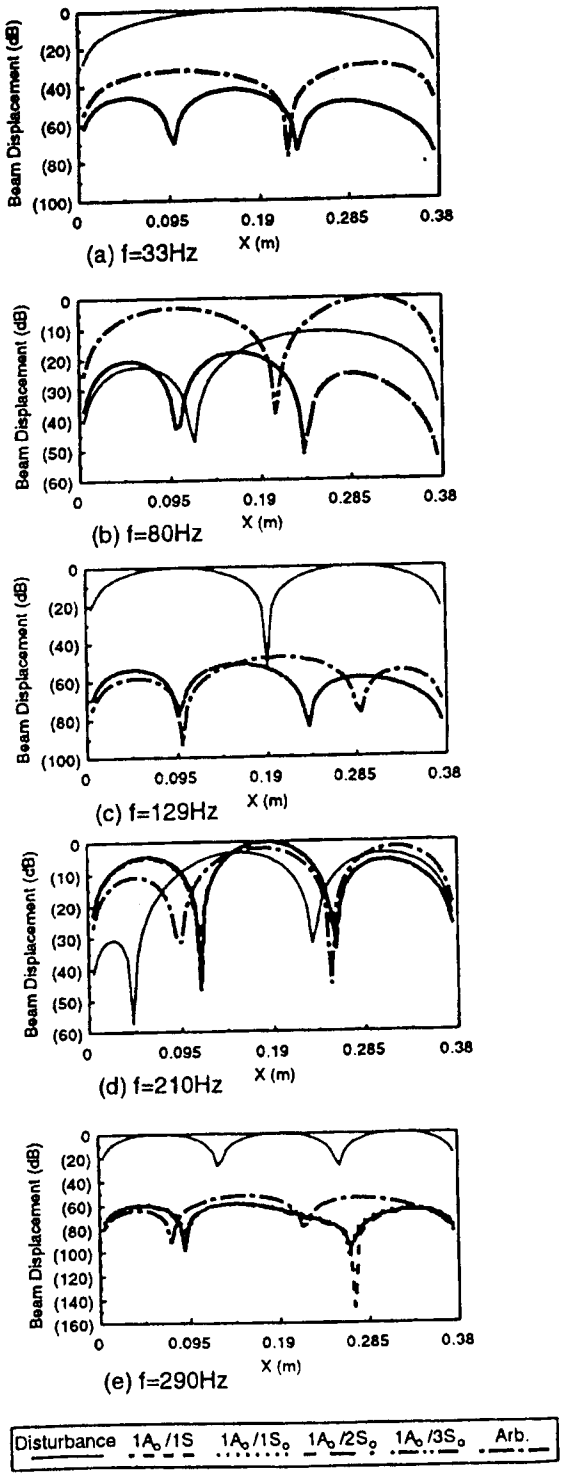

FIG. 6. Beam displacement distributions.

Control voltages of the PZT actuators (volts rms).

Excitation frequency (Hz)	$1A_0/1S$	$1A_0/1S_0$	$1A_0/2S_0$	$1A_0/3S_0$	Arb.
33	52.78	52.78	52.78	53.78	103.68
80	45.73	45.82	45.66	45.76	111.28
129	34.49	34.49	34.49	34.49	26.26
210	20.08	20.48	21.34	21.15	8.75
290	17.79	17.79	17.79	17.79	11.93

duced. In particular, for off-resonance excitation cases only the wave-number components in the supersonic region are reduced, and spillover occurs in the subsonic region. This can explain the control mechanism discussed previously. The significant radiation modes, which are generally the lower modes, are reduced leaving the less significant radiation modes such as the higher modes. Since only those wave-number components in the supersonic region contribute to the far-field sound radiation, it is reasonable to note that in order to efficiently control the structural sound radiation one should reduce the wave-number components in the supersonic region. The wave-number domain controller was discussed by Fuller and Burdisso[43] and experimentally verified.[44,45]

Table VI summarizes the control voltages input to PZT actuators for optimal control of sound radiation from the beam. One can observe that the optimally located PZT actuators require much less control voltages than the arbitrarily selected ones for 33- and 80-Hz excitation. The control effort decreases as the excitation frequency increases, because the lower modes are generally the most efficient radiator and require larger control effort. It is interesting to note that the control voltages are almost the same for applying different numbers of microphones in conjunction with the use of one optimally located PZT actuator. When the optimally located PZT actuator is fixed, the location and number of microphone sensors will not affect the control voltages required for the PZT actuator. However, the location and number of microphone sensors do affect the sound radiation characteristics as shown previously.

IV. CONCLUSIONS

This work analytically shows the performance of optimally positioned PZT actuators and microphone sensors in active structural acoustic control. A simply supported beam in an infinite rigid baffle subjected to a harmonic point force is considered. While the microphones located in the far-field are used as the error sensors, the PZT actuators directly attached to the beam applied as active control forces in conjunction with the use of LMS feedforward control algorithm. A solution strategy with the adoption of the GA incorporated with the LQOCT to calculate the control voltages to the actuators is proposed to determine the optimal locations of PZT actuators and microphone sensors. Their optimal locations can be successfully obtained by the proposed solution strategy. Results show that the optimally positioned actuators and sensors can perform better sound radiation control than the arbitrarily selected ones. In partieular, for off-resonance excitation cases the optimized actuators and sensors can eliminate control spillover. The effect of the number of microphone sensors are also studied. The control mechanisms of optimized PZT actuators and far-field microphone sensors are demonstrated through the radiation directivity patterns and beam displacement distributions as well as the wave-number analysis. The use of the optimally positioned PZT actuators and microphone sensors can efficiently achieve

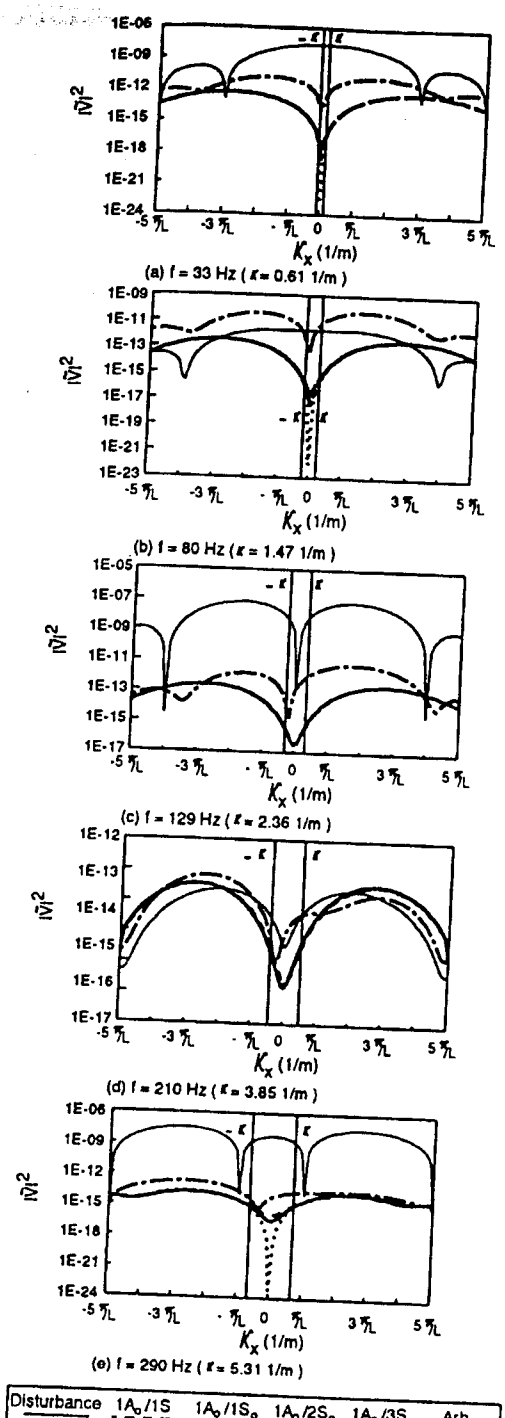

FIG. 7. Mean square values of velocity transform.

structural sound radiation control. The proposed optimization technique can be applied to other active control systems for optimally positioning actuators and sensors.

ACKNOWLEDGMENTS

The author gratefully acknowledges the support of the work by National Science Council, Republic of China, under grant NSC83-0401-E-020-008.

[1]C. R. Fuller, "Active Control of Sound Transmission/Radiation from Elastic Plates by Vibration Inputs, I: Analysis," J. Sound. Vib. **136**, 1–15 (1990).

[2]V. L. Metcalf, C. R. Fuller, R. J. Silcox, and D. E. Brown, "Active Control of Sound Transmission/Radiation from Elastic Plates by Vibration Inputs—II Experiments," J. Sound Vib. **153**, 387–402 (1992).

[3]R. L. Clark and C. R. Fuller, "Experiments on Active Control of Structurally Radiated Sound Using Multiple Piezoceramic Actuators," J. Acoust. Soc. Am. **91**, 3313–3320 (1992).

[4]B. T. Wang, C. R. Fuller, and E. K. Dimitriadis, "Active Control of Structurally Radiated Noise Using Multiple Piezoelectric Actuators," AIAA J. **29**, 1802–1809 (1991).

[5]C. R. Fuller, C. H. Hansen, and S. D. Snyder, "Experiments on the Active Control of Sound Radiation from a Panel Using a Piezoceramic Actuators," J. Sound Vib. **150**, 179–190 (1991).

[6]R. J. Silcox, H. C. Lester, and S. B. Abler, "An Evaluation of Active Noise Control in a Cylindrical Shell," J. Vib. Acoust. Stress Reliability Design **111**, 337–342 (1989).

[7]J. Pan and C. H. Hansen, "Active Control of Noise Transmission Through a Panel into a Cavity, III: Effect of the Actuator Location," J. Acoust. Soc. Am. **90**, 1493–1501 (1991).

[8]C. Deffayet and P. A. Nelson, "Active Control of Low Frequency Harmonic Sound Radiated by a Finite Panel," J. Acoust. Soc. Am. **84**, 2192–2199 (1988).

[9]C. H. Jo and S. J. Elliott, "Active Control of Low-Frequency Sound Transmission Between Rooms," J. Acoust. Soc. Am. **92**, 1461–1472 (1992).

[10]H. C. Lester and C. R. Fuller, "Active Control of Propeller Induced Noise Fields Inside a Flexible Cylinder," AIAA J. **28**, 1374–1380 (1990).

[11]R. A. Burdisso and C. R. Fuller, "Dynamic Behavior of Structural-Acoustic Systems in Feedforward Control of Sound Radiation," J. Acoust. Soc. Am. **92**, 277–286 (1992).

[12]S. D. Snyder and N. Tanaka, "On Feedforward Active Control of Sound and Vibration Using Vibration Error Signals," J. Acoust. Soc. Am. **94**, 2181–2193 (1993).

[13]K. Naghshineh, "Active Control of Sound Power Using Acoustic Basis Functions as Surface Velocity Filters," J. Acoust. Soc. Am. **93**, 2740–2752 (1993).

[14]R. L. Clark and C. R. Fuller, "Modal Sensing of Efficient Acoustic Radiators with PVDF Distributed Sensors in Active Structural Acoustic Approaches," J. Acoust. Soc. Am. **91**, 3321–3329 (1992).

[15]R. L. Clark and C. R. Fuller, "Active Structural Acoustic Control with Adaptive Structures Including Wavenumber Considerations," J. Intell. Mat. Syst. Struct. **2**, 431–452 (1992).

[16]R. L. Clark, R. A. Burdisso, and C. R. Fuller, "Design Approaches for Shaping Polyvinylidene Fluoride Sensors in Active Structural Acoustic Control (ASAC)," J. Intell. Mat. Syst. Struct. **4**, 354–365 (1993).

[17]R. L. Clark and C. R. Fuller, "Control of Sound Radiation with Adaptive Structures," J. Intell. Mat. Syst. Struct. **2**, 431–452 (1991).

[18]R. L. Clark, C. R. Fuller, B. R. Fogg, and W. V. Miller, "Structural Acoustic Control Using Optical Fiber Sensors and Piezoelectric Actuators," in *Proceedings of the International Symposium and Exhibition on Active Materials and Adaptive Structures*, Alexandria, Virginia (Technomic, Lancaster, PA, 1991).

[19]C. R. Fuller and J. D. Jones, "Influence of Sensor and Actuator Location on the Performance of Active Control Systems," presented at the ASME Winter Annual Meeting, 87-WA/NCA-9, 1987.

[20]A. J. Bullmore, P. A. Nelson, A. R. D. Curtis, and S. J. Elliott, "The Active Minimization of Harmonic Enclosed Sound Fields, Part II: A Computer Simulation," J. Sound Vib. **117**, 15–33 (1987).

[21]R. E. Lindberg, Jr. and R. W. Longman, "On the Number and Placement of Actuators for Independent Modal Space Control," J. Guidance Control **7**, 215–221 (1984).

[22]G. A. Norris and R. E. Skelton, "Selection of Dynamic Sensors and Actuators in the Control of Linear System," J. Dynamic Syst., Meas. Control **111**, 389–397 (1989).

[23]B. T. Wang, R. A. Burdisso, and C. R. Fuller, "Optimal Placement of Piezoelectric Actuators for Active Structural Acoustic Control," J. Intell. Mat. Syst. Struct. **5**, 67–77 (1994).

[24]R. L. Clark and C. R. Fuller, "Optimal Placement of Piezoelectric Actuators and Polyvinylidene Fluoride Error Sensors in Active Structural Acoustic Control Approaches," J. Acoust. Soc. Am. **92**, 1521–1533 (1992).

[25]E. F. Crawley and J. de Luis, "Use of Piezoelectric Actuators as Elements of Intelligent Structures," AIAA J. **25**, 1373–1385 (1987).

[26]T. Bailey and J. E. Hubbard, "Distributed Piezoelectric-Polymer Active Vibration Control of a Cantilevered Beam," J. Guidance Control **6**, 605–611 (1986).

[27]C. K. Lee and F. C. Moon, "Modal Sensors/Actuators," J. Appl. Mech. **57**, 434–441 (1990).

[28]E. K. Dimitriadis, C. R. Fuller, and C. A. Rogers, "Piezoelectric Actuators for Distributed Vibration Excitation of Thin Plate," J. Vib. Acoust. **113**, 100–107 (1991).

[29]B. T. Wang, "The Performance of Accelerometers and PVDF Sensors in Active Structural Vibration Control," Bull. Natl. Pingtung Poly. Inst. **3**, 81–92 (1994).

[30]B. T. Wang and C. R. Fuller, "Near-Field Pressure, Intensity, and Wave-Number Distributions for Active Structural Acoustic Control of Plate Radiation: Theoretical Analysis," J. Acoust. Soc. Am. **92**, 1489–1498 (1992).

[31]B. T. Wang, "Active Control of Far-Field Sound Radiation by a Beam with Piezoelectric Control Transducers: Physical System Analysis," Smart Mater. Struct. **3**, 476–484 (1994).

[32]J. Jia, "Optimization of Piezoelectric Actuator Design in Vibration Control Systems," Ph.D. thesis, Department of Mechanical Engineering, Virginia Polytechnic Institute and State University, 1990.

[33]D. E. Goldberg, *Genetic Algorithms in Search, Optimization and Machine Learning* (Addison-Wesley, Reading, MA, 1989).

[34]W. M. Jenkins, "Structural Optimisation with the Genetic Algorithm," Struct. Eng. **69**, 418–422 (1991).

[35]R. L. Riche and R. T. Haftka, "Optimization of Laminate Stacking Sequence for Buckling Load Maximization by Genetic Algorithm," AIAA J. **31**, 951–956 (1993).

[36]B. T. Wang, "Application of Genetic Algorithms to the Optimum Design of Active Control Systems," Proceedings of International Noise and Vibration Control Conference 231–236 (1994).

[37]C. E. Wallace, "Radiation Resistance of a Baffled Beam," J. Acoust. Soc. Am. **51**, 936–945 (1972).

[38]B. T. Wang and C. A. Rogers, "Modeling of Finite-Length Spatially Distributed Induced Strain Actuators for Laminate Beams Structures," J. Intell. Mat. Syst. Struct. **2**, 38–58 (1991).

[39]F. Fahy, *Sound and Structural Vibration* (Academic, Orlando, FL, 1985).

[40]B. T. Wang, "A Dynamic Simulation of Hybrid Active and Passive Control of Structural Vibration" (NSC Report: NSC 81-0401-E-020-501, Republic of China, 1992).

[41]B. T. Wang, "Application of Genetic Algorithm to the Design of Intelligent Material Structure System" (NSC Report: NSC83-0401-E-020-008, Republic of China, 1994).

[42]Inc. Piezo Systems, *Product Catalog* (1990).

[43]C. R. Fuller and R. A. Burdisso, "A Wavenumber Domain Approach to the Active Control of Structure-borne Sound," J. Sound Vib. **148**, 355–360 (1991).

[44]J. P. Maillard and C. R. Fuller, "Advanced Time Domain Wave-Number Sensing for Structural Acoustic Systems: I. Theory and Design," J. Acoust. Soc. Am. **95**, 3252–3261 (1994).

[45]J. P. Maillard and C. R. Fuller, "Advanced Time Domain Wave-Number Sensing for Structural Acoustic Systems: II. Active Radiation Control of a Simply Supported Beam," J. Acoust. Soc. Am. **95**, 3262–3272 (1994).